RSC Advances

PAPER

View Article Online
View Journal | View Issue

Cite this: *RSC Adv.*, 2026, **16**, 8154

Electrochemical evaluation of low-cost flexible supercapacitors based on nickel-coated activated carbon textile electrodes

Paola G. Vilchis-Gutiérrez,[ab] José A. Ávila-Niño,*[c] Ma. Dolores Durán-García,*[a] Marquidia J. Pacheco-Pacheco[d] and Iván G. Martínez-Cienfuegos[a]

This study presents the development of low-cost flexible supercapacitors (SCs) based on cotton textile electrodes impregnated with activated carbon (AC) and coated with nickel *via* sputtering. The electrochemical performance was optimized by varying the activated carbon (AC) ink immersion cycles (1, 3, and 5 immersions, corresponding to 0.0727, 0.2041, and 0.2936 grams, respectively) and the sputtered nickel amount (0.011, 0.002, 0.0029, and 0.0032 grams corresponding to 1, 3, 10 and 15 minutes of deposition, respectively). We found that a moderate nickel deposition improved electron transport and reduced charge transfer resistance, while excessive deposition can block pores and decrease capacitance, nevertheless the presence of nickel improves the stability of the device, for example, the configuration of the electrodes with 0.2041 g of AC and 0.002 g of Ni shows a specific capacitance of 382.40 mF cm^{-2} (at 5 mV s^{-1}) and a high stability (95.76%) after 1000 cycles. These findings demonstrate that balancing carbon and nickel coating content is a critical parameter for the good electrochemical performance of SCs. This work advances the design of flexible, lightweight, and wearable supercapacitors, paving the way for high-performance and sustainable energy solutions for portable electronics and sustainable energy storage.

Received 23rd December 2025
Accepted 26th January 2026

DOI: 10.1039/d5ra09914e

rsc.li/rsc-advances

Introduction

The global demand for sustainable energy solutions has accelerated the development of advanced electrochemical energy storage technologies. Among these, supercapacitors (SCs) stand out for their high-power density, rapid charge–discharge capability, and long cycle life, making them ideal for applications in electric vehicles, portable electronics, and wearable devices. Flexible SCs have gained particular attention due to their potential integration into textiles and wearable systems. Recent advancements have explored high-performance materials such as MXene-based composites, polymer gel electrolytes, and hybrid carbon-metal structures, achieving notable improvements in capacitance and stability.[1] However, many of these approaches involve complex fabrication processes and high costs, limiting their scalability and accessibility.

Textiles made from natural or synthetic fibres have evolved with the development of functional cotton fabrics, enabling the creation of SC prototypes in textile fibres for energy storage. These materials diversify substrate options for flexible devices, opening new possibilities in the field of wearable and energy storage technology.[2–4]

The electrochemical performance of nickel-coated activated carbon SCs is an emerging field that combines the benefits of advanced materials such as activated carbon and nickel for enhanced energy storage applications;[5] nickel is chosen due to its high theoretical specific capacitance, high reserves, and low cost. When used as a coating on activated carbon electrodes, nickel forms an efficient composite that leverages the cyclic stability and general performance of SCs.[6] Using nickel-coated textiles also introduces flexibility and lightweight properties, making them suitable for wearable and portable energy storage devices.[7,8]

Activated carbon is a preferred material for supercapacitor applications due to its high surface area, excellent conductivity, and ability to support double-layer capacitance.[9,10] Nickel-based electrodes, such as nickel hydroxide or nickel oxide, have been shown to provide enhanced energy storage due to their ability to undergo reversible faradaic reactions, making them ideal for hybrid SCs.[11]

In this work, we propose a novel and accessible alternative: cotton textile electrodes impregnated with activated carbon and

[a]*Universidad Autónoma del Estado de México, Cerro de Coatepec s/n, Ciudad Universitaria, Toluca, Estado de México, 50000, Mexico. E-mail: mddurang@uaemex.mx*

[b]*CIDETEQ Centro De Investigación y Desarrollo Tecnológico en Electroquímica, S.C., Parque Tecnológico Querétaro s/n, Pedro Escobedo, Querétaro, 76703, Mexico*

[c]*Secretaría de Ciencia, Humanidades, Tecnología e Innovación (Secihti) – CIATEQ Centro de Tecnología Avanzada, Nodo Servidor Público 165, Anexo al Club de Golf, Las Lomas Zapopan, Jalisco, 45131, Mexico*

[d]*Instituto Nacional de Investigaciones Nucleares, Carretera México Toluca-La Marquesa s/n, Ocoyoacac, Estado de México, 52750, Mexico*

coated with nickel *via* sputtering. Cotton offers a flexible, low-cost, and abundant substrate, while activated carbon provides high surface area and excellent conductivity. Nickel enhances electrochemical performance by improving conductivity and stability, provided its deposition is carefully controlled to avoid pore blockage.

Using a simple and reproducible dipping–impregnation and sputtering method, 45 SC prototypes were fabricated and characterized. Key parameters such as specific capacitance, energy density, internal resistance, and cyclic stability were evaluated. The results demonstrate competitive performance compared to state-of-the-art flexible SCs, positioning this approach as a viable solution for scalable, sustainable, and high-performance energy storage in wearable electronics.

Nickel-coated activated carbon textile electrodes represent a promising direction in developing high-performance SCs. By optimizing the interaction between nickel and activated carbon, researchers aim to enhance the electrochemical properties of these devices, making them suitable for various applications, from portable electronics to electric vehicles.[12,13]

The novelty of this work lies in the systematic optimization of cotton-based textile electrodes impregnated with activated carbon and coated with nickel by sputtering. Unlike previous reports that focused on carbon nanotube yarns or complex fibre processing routes, our approach employs an abundant, low-cost cotton substrate combined with a simple dipping-impregnation and sputtering method. This strategy enables precise control of both carbon loading and nickel thickness, allowing us to correlate surface area, conductivity, and capacitance with fabrication parameters. The resulting devices achieve competitive areal capacitances and excellent cycling stability while maintaining methodological simplicity and scalability. These features distinguish our study from earlier Ni–carbon textile electrodes and highlight its potential for affordable, flexible, and wearable energy storage applications.

Materials and methods

The main goal of this research is to characterize the electrochemical performance of carbon-nickel textile SCs. This includes everything from its design to leveraging the unique properties of cotton fabric as a substrate and AC as an electrode material. AC was chosen due to its high surface area and favourable electrochemical properties, and nickel was selected as an additive to improve the conductivity and stability of the device. A methodological approach has been employed, ranging from the selection and preparation of materials to the characterization and evaluation of the electrochemical properties of the manufactured supercapacitors.

The synthesis and preparation of the SC components involved detailed methodologies, including substrate preparation, carbon treatment, nickel deposition, and device assembly. The process also incorporated advanced characterization techniques, such as scanning electron microscopy (SEM), energy dispersive spectroscopy (EDS), cyclic voltammetry (CV), galvanostatic charge–discharge (GCD), and electrochemical impedance spectroscopy (EIS), to evaluate the physical, chemical, and electrochemical properties of the materials and devices. The experimental procedure examined various combinations of key factors, including the number of immersions in activated carbon ink and nickel deposition times. To ensure the reliability of the findings, all tests were conducted in triplicate, yielding 45 supercapacitor prototypes. The electrode fabrication process followed the methodology established in previous research.[14]

Supercapacitor configuration

Substrate preparation. In the present work, considering the proposals by Liu *et al.* and Wang *et al.*,[3,15] we previously washed the cotton fabric substrates to remove impurities, mainly fats, using a non-ionic biodegradable detergent and dried them at room temperature before cutting them to a size of 5 cm × 5 cm. Then, cotton substrates were immersed in a solution of ethanol/deionized water in a 3 : 2 ratio, using 300 mL of ethanol and 200 mL of water, and then subjected to an ultrasonic bath for 20 minutes. It was then dried in a natural convection oven at 110 °C for 20 minutes on each side, and its mass was recorded using an analytical balance.

Synthesis of activated carbon ink. The activated carbon ink synthesis was made using ground AC powder—Sigma-Aldrich® brand activated carbon, which was subjected to 40 hours of mechanical grinding to reduce the grain size and thus have better adhesion to the cotton fabric and optimal diffusion in the solution (ink)—, deionized water as a solvent, and dodecylbenzene sodium sulfonate (DBSS) as a surfactant to homogeneously disperse the activated carbon particles and promote their impregnation into the cotton fibres, to enhancing coating uniformity and wetting, without directly contributing to capacitance;[16–18] then, an activated carbon ink was made from 4 grams of AC and 1 g of DBSS, dissolved in 50 mL of deionized water, which was subjected to an hour of ultrasonic bath.

Impregnation of ink on the substrate. The pieces of cotton fabric were immersed in the ink and placed in an ultrasonic bath for 30 minutes, after which they were placed in an oven for 15 minutes per side at 110 °C to remove moisture, repeating the process once, three, and five times.

Nickel coating synthesis. Nickel deposition was performed using magnetron sputtering. Several authors used this technique in textile fibres.[16,19] In the present work, a nickel coating was deposited on cotton textile fibre substrates impregnated with activated carbon ink by sputtering. A nickel plate was used as a target, and the process was carried out in an argon atmosphere at 150 W for 15, 10, 3, and 1 minutes, to compare the electrochemical behaviour of electrodes containing different amounts of this metal in their structure. To deposit a Ni thin film on cotton substrates impregnated with AC, sputtering equipment was used. A fixed power of 150 Watts was applied, in an argon atmosphere at approximately 2.5×10^{-2} Torr, reaching a temperature of roughly 40 °C.

Supercapacitor prototype assembly. Textile electrodes were cut into 2-cm diameter circle disks. A filter separator of mixed cellulose esters (Merk Millipore membrane 0.45 μm pore size, 150 μm thick) and an aqueous 1 M KOH electrolyte were used. For the SC assembly, two stainless steel disks were used as

current collectors using a stainless-steel cell to press the electrodes and guarantee the contact between the current collectors and the electrodes.

For the flexible prototype, two aluminium foil sheets in contact with the electrodes served as current collectors, and the SC was then encapsulated within a polypropylene package, using the electrolyte solution containing poly (vinyl alcohol) to form a KOH : PVA (1 : 1) gel.

Experimental design

Fifteen prototypes were obtained and measured three times (45 in total); error bars were included by using standard deviations. The combination of AC immersions and Ni depositions yields the following electrodes: the 1C electrodes (1 AC immersion) with varying Ni sputtering times: 1C + 0Ni, 1C + 1Ni, 1C + 3Ni, 1C + 10Ni, and 1C + 15Ni, corresponding to Ni depositions of 0, 1, 3, 10, and 15 minutes, respectively. The same nomenclature was repeated for the electrodes with 3 AC immersions (3C + 0 Ni, 3C + 1Ni, 3C + 3Ni, 3C + 10Ni, and 3C + 15 Ni), and for 5 AC immersions (5C + 0 Ni, 5C + 1Ni, 5C + 3Ni, 5C + 10Ni, and 5C + 15 Ni).

Physicochemical characterization of the SCs yielded key results for the electrodes. SEM was performed to observe and quantify the elements present in the electrodes. Further characterization of the electrodes was performed by measuring their thickness, weight, and electrical conductivity, the latter measured using a four-point probe technique with a Keithley B2902A Source Measure Unit. The Brunauer–Emmett–Teller (BET) specific surface area and pore width were determined with an Autosorb iQ. Surface area and pore width were calculated according to the Dubinin–Radushevich (DR) method,[20] as they are key parameters in evaluating the surface area of the electrodes due to the carbon impregnation of the cotton substrates and due to Ni incorporation by sputtering.

Electrochemical characterization was performed using a SP-150 Biologic potentiostat. The equations for obtaining capacitance by CV and GCD techniques, energy, and power densities are described below:

Capacitance from CV: $C_{CV} = \frac{\int I dt}{2\nu a \Delta v}$, where I is the constant current, t is time, ν is the scan rate, a is the active area of the electrode, and ΔV is the potential window.

From GCD, capacitance is calculated as follows: $C_{GCD} = \frac{I\Delta t}{a\Delta V}$, where I is the discharge current, a is the area of the active material, ΔV is the voltage window, and Δt is the discharge time.[21]

Energy density was calculated following the equation $E = \frac{1}{2}C_T(\Delta V)^2$, while power density $P = \frac{E}{\Delta t}$, where E and P are energy and power densities, and C_T is the total capacitance.[21]

Results and discussion

BET data (Tables 1 and 2) show that the surface area increases with carbon loading (1C → 3C → 5C) and generally decreases with nickel deposition. It is inferred that Nickel particles may partially block the pores or cause some densification of the material, leading to a reduced surface area, which is consistent with the results obtained by Tai *et al.*[22] for Ni-coated polyacrylonitrile-based activated carbon fabric electrodes for SCs. For example, tests on electrode 5C + 0Ni show the highest surface area due to its unblocked, porous structure, which maximizes potential adsorption sites.

Table 1 BET analysis for different carbon content electrodes

Electrode	Surface area [$m^2\ g^{-1}$]
1C + 0Ni	188.41
3C + 0Ni	243.05
5C + 0Ni	360.09

Table 2 BET analysis for different nickel content electrodes

Electrode	Surface area [$m^2\ g^{-1}$]
5C + 1Ni	310.83
5C + 3Ni	331.72
5C + 10Ni	161.81
5C + 15Ni	146.12

Conversely, nickel deposition on the electrodes (5C + 1Ni, 5C + 3Ni, *etc.*) results in a progressive decrease in surface area, reaching its lowest value in the 5C + 15Ni electrode (146.12 $m^2\ g^{-1}$). However, the 5C + 3Ni electrode is an exception, showing a slight increase in surface area. This tendency supports the idea that Ni particles may infiltrate or coat the carbon porous network, causing pore blockage. Consequently, Ni deposition limits the electrode's capacity for applications on high surface areas, such as in SCs. However, as it can be shown below in this work, there are special electrode configurations where Ni could enhance the specific capacitance of the SCs and also improve the cyclic stability and the resistance of the electrode, making moderate Ni adhesion a good approach to enhance the SC electrochemical performance.

We found that sheet resistance decreases monotonically with both AC impregnation cycles and metallic Ni deposition, indicating improved electron transport pathways (Fig. 1). In a previous work, we found that XRD spectrum of this type of electrode shows a Ni (111) peak consistent with metallic Ni presence at low thickness on AC-cotton.[14]

Then, Ni addition enhances the electrical conductivity of the electrode, meaning that the presence of nickel appears to improve electron transport within the electrode. The trend for electrodes containing most Ni confirms that nickel significantly reduces electrical resistance across different carbon concentrations.

Throughout this paper, the effect of carbon ink immersions on electrodes with a constant nickel content was investigated. It was observed that increasing the carbon content tends to reduce the sheet resistance. This fact suggests that a higher carbon content contributes to better conductivity, possibly due to a more interconnected conductive network within the material.

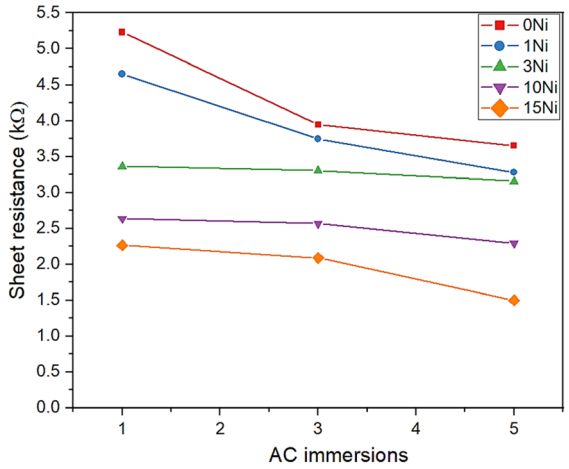

Fig. 1 Sheet resistance *vs.* AC immersions.

Table 3 Weights and thicknesses of AC-Ni textile electrodes

Sputtering time (min)	1	3	10	15
Weight (g)	0.0011	0.002	0.0029	0.0032
Thickness (nm)	14.06	78.9	142.53	366.3

Table 3 shows the weights and thicknesses of the nickel deposit onto the AC-Ni textile electrodes for each of the sputtering time. Specific capacitances were obtained for each prototype in triplicate to ensure the reliability of the results.

Cyclic voltammetry (CV) curves reveal that the incorporation of nickel significantly modifies the capacitive response of the cotton-AC electrodes (Fig. 2).

The specific capacitance decreases progressively with increasing scan rate for all samples (Fig. 2), a behavior attributed to the limited accessibility of the electrolyte to the inner pores at high sweep speeds. Among the tested configurations, the 5C + 0Ni prototype consistently exhibits the highest capacitance values across all scan rates, followed by 3C + 0Ni and 1C + 0Ni. At low scan rates, the advantage of the 5C + 0Ni electrode becomes particularly evident; for example, at 5 mV s^{-1} it reaches 551 mF cm^{-2}, reflecting a superior energy storage capacity compared to the other prototypes. This trend is consistent with the increased surface area resulting from higher activated carbon loading, confirming the direct correlation between immersion cycles and accessible porosity for charge storage.

SCs subjected to a single AC ink immersion are shown in Fig. 2(b), where it is observed that the 1C + 1Ni SC has the highest specific capacitance value at all scanning rates (109.16

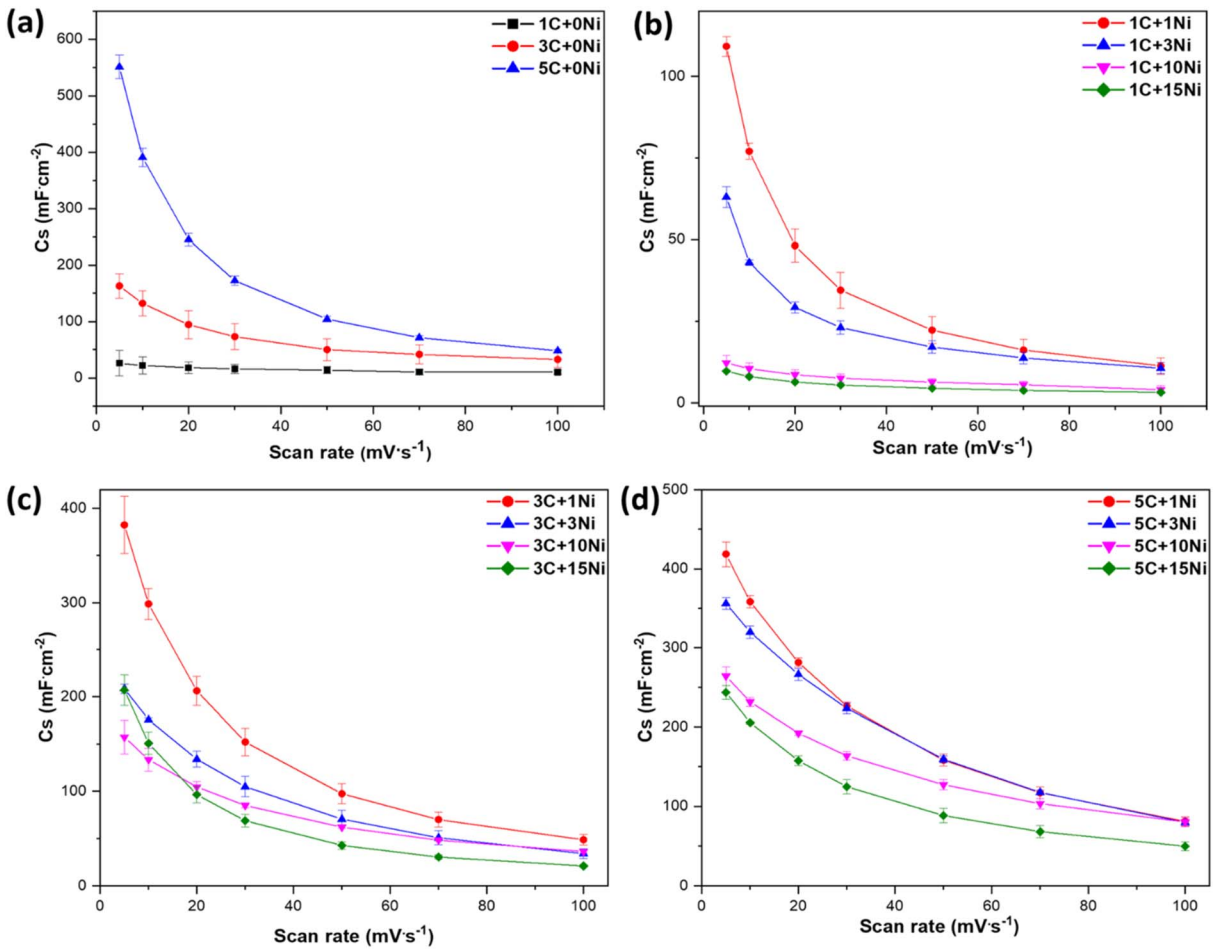

Fig. 2 Specific capacitance *vs.* scan rate obtained by CV: (a) electrodes with different load of C without Ni, (b) 1C electrodes, (c) 3C electrodes, (d) 5C electrodes.

mF cm^{-2} at 5 mV s^{-1}), followed by 1C + 3Ni (63.05 mF cm^{-2} at 5 mV s^{-1}). The prototypes subjected to 10 and 15 minutes of Ni sputtering showed lower C_s values compared to the other characterized prototypes. Adding a moderate amount of nickel (1Ni and 3Ni) appears to improve C_s than 1C + 0Ni, but higher amounts of nickel reduce the C_s of the devices.

Fig. 2(c) denotes the SCs with 3 AC immersions, the 3C + 1Ni prototype has the highest value of C_s (382.40 mF cm^{-2} at 5 mV s^{-1}), followed by 3C + 3Ni (208.46 mF cm^{-2} at 5 mV s^{-1}); it is observed that the Cs decreases significantly for 3C + 10Ni and 3C + 15Ni, similar trend observed in 2(b). In summary, for 1C and 3C SCs, a moderate amount of nickel improves Cs, but higher amounts reduce this characteristic.

This behavior has been observed by other authors for electrodes containing Ni or Ni-based compounds and carbon,[19,22–25] including Tai *et al.*,[22] who found that the capacitance of Ni–C SCs diminishes by adding Ni coating after achieving a capacitance peak for low Ni load, arguing that for higher Ni content, the pore access are blocked, reducing in the same manner the electrode surface. For a moderate amount of Ni, the capacitance is improved, probably by the change of the surface polarity on the carbon surface, enhancing the affinity of OH^- species from the electrolyte solution,[22] and promoting a better interaction between the electrolyte and the carbon electrode, which is consistent with the reduction of the charge transfer resistance as reported below and in a previous work.[14]

The importance of presenting areal-specific capacitance instead of gravimetric-specific capacitance is because when Ni is added to the carbon-based electrode, the relative mass of the active material decreases, and the total capacitance of the composite also decreases.[26]

For those electrodes with the highest amount of carbon in their structure, the capacitance results are shown in Fig. 2(d), where it is of interest that the electrode with 5 immersions and absence of nickel (5C + 0Ni) has the highest specific capacitance at all scanning speeds; 5C + 3Ni and 5C + 1Ni have slightly higher C_s values compared to the SCs with higher Ni content, but still lower than 5C + 0Ni. This can be attributed to carbon's ability to store energy, and the fact that more material improves capacitance. Compared to carbon electrodes with 1 and 3 immersions, the high active area resulting from 5 AC ink immersions is altered to a greater extent by Ni addition, where a small amount of Ni is sufficient to decrease capacitance due to the reduction of surface area, as shown below.

Specific capacitance values were also obtained by the GCD technique for each of the electrodes (Fig. S3–S5). Fig. 3 shows

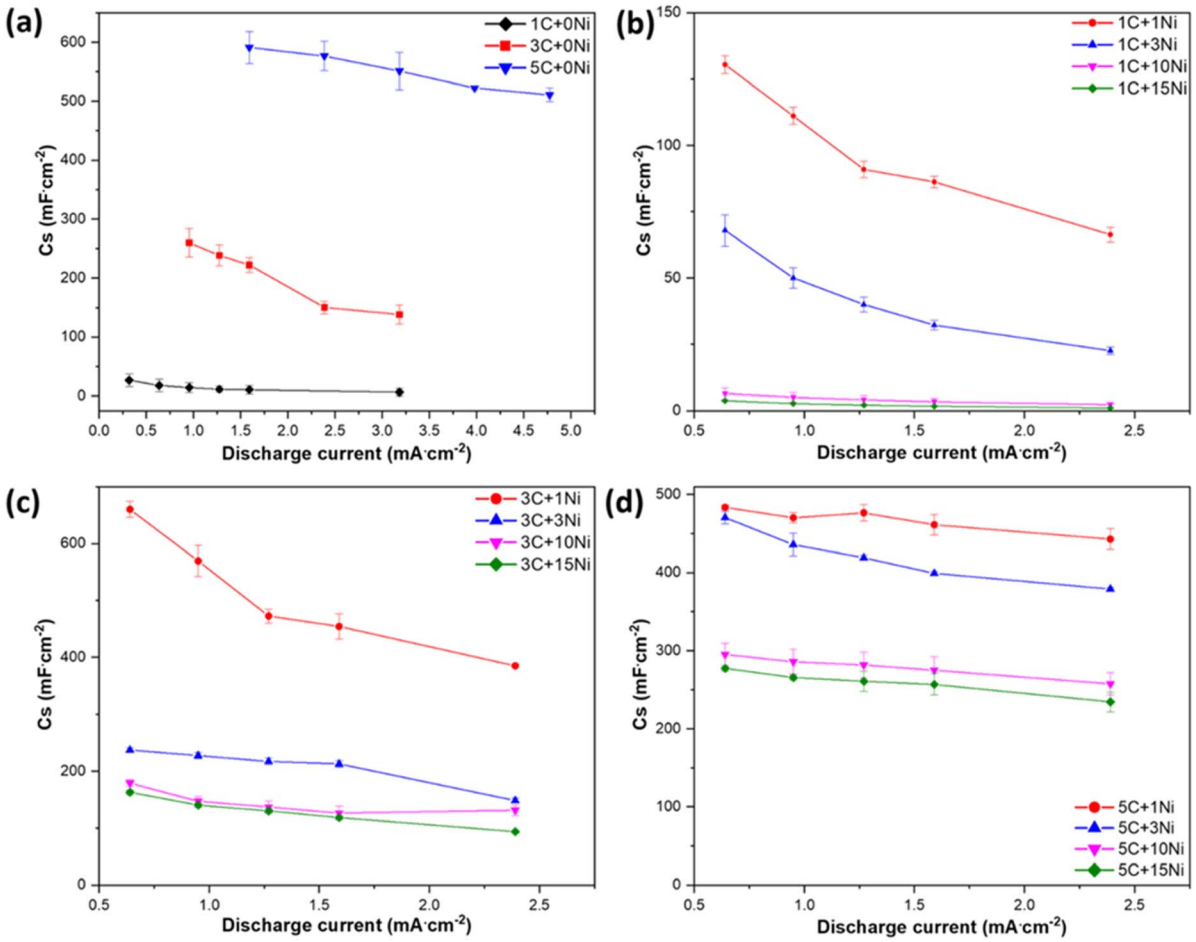

Fig. 3 Specific capacitance *vs.* discharge current for: (a) electrodes with different load of C without Ni, (b) 1C electrodes, (c) 3C electrodes, (d) 5C electrodes.

that the behavior of the capacitance obtained from cyclic voltammetry curves is maintained for this technique. Fig. 3(a) shows the C_s of SCs without Ni, with more AC ink immersions yielding higher capacitance.

The behavior observed in Fig. 3 is similar to that presented in the CV results, as shown in Fig. 3(b), where prototype electrodes with 1 AC immersion and 1C + 1Ni SCs have the highest C_s at all applied currents, followed by 1C + 3Ni. SCs with a higher amount of Ni (10 and 15 min) exhibit similar and lower specific capacitances compared to the other SCs. The nickel-free prototype (1C + 0Ni) has a very low C_s value, indicating that the moderate addition of nickel improves this parameter.

Regarding the 3C + 3Ni and 3C + 1Ni prototypes (Fig. 3(c)), they exhibit the highest C_s values, indicating that the addition of nickel improves the C_s to a certain extent. However, at a higher nickel amount, storage capacitance decreases.

As observed in the CV measurements, the C_s for the SCs with 5 AC ink immersions diminish when Ni content increases (Fig. 3(d). Fig. 4(a–c) summarizes the comparison between these techniques using those values corresponding to a sweep rate of 5 mV s^{-1} (CV) and a current of 1.59 mA cm^{-2} (GCD) of all the prototypes.

From the results obtained by GCD, it is possible to calculate the values of energy density (Wh cm^{-2}) and power density (W cm^{-2}). These values were obtained for all the prototypes, shown in Fig. 4(d–f). The relationship between these densities is commonly known as a Ragone plot.

Fig. 4(d), which shows the results for 1C, indicates that 1C + 3Ni has the highest energy density at all power densities, followed by 1C + 1Ni. In contrast, devices with 1C + 10Ni and 1C + 15Ni exhibit lower energy densities.

For the SCs with 3 carbon immersions, shown in Fig. 4(e), the SC with a nickel coating of 1 minute (3C + 1Ni) has the highest energy density at all power densities, followed by 3C + 3Ni, and after these, the SCs with the highest nickel content, showing higher nickel level reduces energy density.

Fig. 4(f) shows how energy density decreases significantly with higher concentrations of nickel (10 and 15 Ni), while lower concentrations of nickel maintain a better energy density.

In the case of the 5C electrodes, which have higher porosity, a small amount of Ni was sufficient to reduce both the specific power and density and C_s.

Fig. 5(a) illustrates the relationship between surface area, pore width, and capacitance density. The graph illustrates the correlation between surface area (black squares) , pore width (red circles) and capacitance density for electrodes containing 1C, 3C, and 5C. It is shown that surface area increases as the capacitance density increases, while pore width decreases slightly. For 5C SCs, a higher capacitance density corresponds to a larger surface area and a narrower pore width.

Fig. 5(b) presents a good relationship between the capacitance (red line) and surface area (black line), suggesting that the

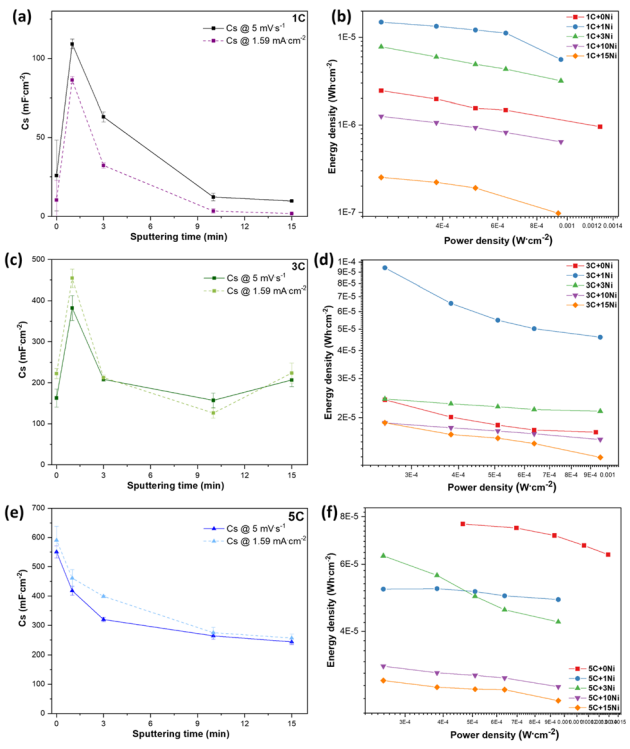

Fig. 4 Specific capacitance *vs.* sputtering time obtained from CV (5 mV s^{-1}) and GCD (1.59 mA cm^{-2}) techniques, and Ragone plots for supercapacitors prepared with 1, 3, and 5 immersion cycles of AC ink. (a) Specific capacitance of 1C SCs as a function of sputtering time, (b) Ragone plot of 1C SCs with different Ni deposition times, (c) specific capacitance of 3C SCs as a function of sputtering time, (d) Ragone plot of 3C SCs with different Ni deposition times, (e) specific capacitance of 5C SCs as a function of sputtering time, and (f) Ragone plot of 5C SCs with different Ni deposition times.

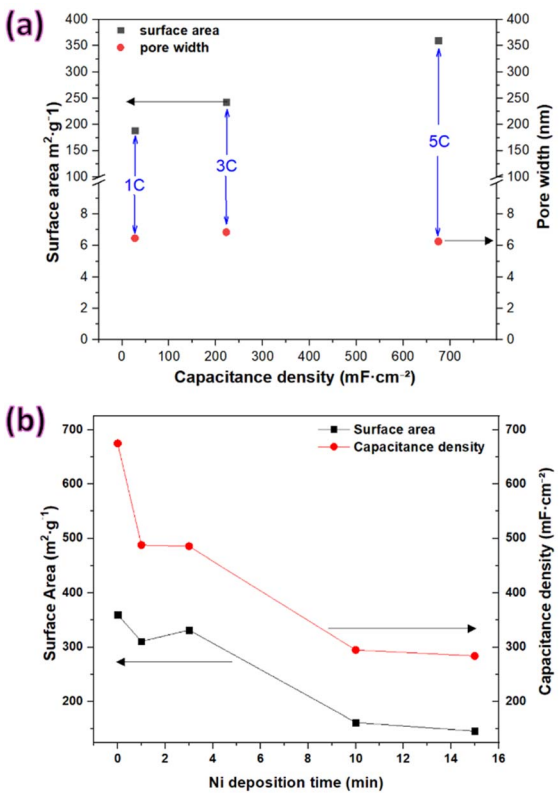

Fig. 5 (a) Influence of C (without Ni) on surface area and capacitance, (b) influence of Ni on surface area and capacitance.

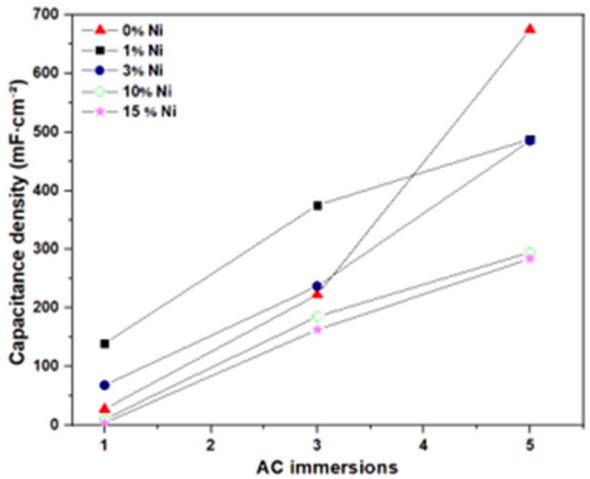

Fig. 6 Effect of nickel deposition time on capacitance density across AC immersions.

surface area is the key parameter for improving the C_s of the SCs.

Fig. 6 illustrates the relationship between capacitance density (mF cm^{-2}) and the number of AC immersions for electrodes with varying nickel (Ni) deposition times. Each line corresponds to a specific deposition time, with different symbols representing each specification. Capacitance increases with the number of AC immersions for all electrodes; those with longer Ni deposition times (10 min and 15 min) exhibit lower increases in capacitance density compared to shorter deposition times (1 min and 3 min).

This fact highlights the impact of nickel deposition time on the capacitive performance, indicating a complex relationship between Ni deposition duration and immersion cycles.

The potential effect of DBSS on electrochemical performance was considered. No redox signals attributable to the surfactant were observed within the applied potential range, confirming that its contribution is indirect, by improving the distribution of activated carbon on the textile.

Table 4 provides a comparative overview of the electrochemical performance of the electrodes developed in this work and those reported in other representative studies from the literature. The analysis focuses on three main aspects:

(a) Superior specific capacitance: the cotton-based electrodes impregnated with activated carbon achieved an exceptionally high areal capacitance of 675.02 mF cm^{-2} (measured by GCD at 1.59 mA cm^{-2}), which surpasses most values reported for similar textile-based supercapacitors, such as oxidized carbon nanotubes (OCNT)-coated yarn (258.47 mF cm^{-2})[16] and C-Web@Ni-cotton fabric (275.8 mF cm^{-2}).[27] This outstanding performance is attributed to the high surface area provided by multiple carbon ink immersions and the effective utilization of the cotton substrate.

(b) Efficient and scalable fabrication: the dipping-impregnation method, combined with sputtering, offers a simple, low-cost, and scalable fabrication route, in contrast to more complex and equipment-intensive techniques. This methodological simplicity makes the proposed approach highly attractive for large-scale production of flexible EE devices.

(c) Robust long-term stability: the electrodes demonstrate excellent cyclic stability, retaining 94% of their initial capacitance after 5000 cycles. This durability is comparable to that of other highly stable materials in the literature, such as the OCNT yarn (92%) and the C-Web@Ni-Cotton fabric (97.4%). This confirms that our material is not only high-performing but also robust and reliable for long-term use.

Electrochemical cycling stability tests highlight the influence of nickel deposition on long-term performance (Fig. 7). The 3C + 0Ni electrode exhibits the lowest stability, with capacitance retention decreasing steadily throughout 1000 cycles. Incorporation of nickel improves this behaviour: the 3C + 1Ni electrode shows higher and more stable retention, although a gradual decline is still observed. In contrast, the 3C + 3Ni configuration demonstrates superior cycling stability, maintaining 95.76% capacitance retention after 1000 cycles, which confirms that higher nickel content enhances durability. This improvement can be attributed to the increased electrical conductivity provided by nickel, which facilitates efficient charge transfer, and to the intrinsic corrosion resistance of Ni, which protects the electrode from degradation during repeated cycling.[25] These findings are consistent with the reduced charge transfer resistance observed in EIS analysis, reinforcing that controlled

Table 4 Comparison with other works in the literature

Electrode materials	Method	Fabrication cost/complexity	Specific capacitance (mF cm^{-2})	Measurement conditions	References
Cotton fabric impregnated with activated carbon	Dipping-impregnation	Low – simple, scalable	675.02 (5C + 0Ni)	1.59 mA cm^{-2} (GCD)	This work
Ni-coated AC-cotton fabric	Dipping-impregnation-sputtering	Medium – requires equipment	487.80 (5C + 1Ni)	1.59 mA cm^{-2} (GCD)	This work
Ni-OCNT-coated cotton yarn	Sputtering	High – complex setup	258.47	1.5 mA cm^{-2} (GCD)	Islam *et al.* 2020 (ref. 16)
Cotton lawn coated with activated carbon	Screen printing	Medium – semi-scalable	430	1 mV s^{-1} (GCD)	Jost *et al.* 2011 (ref. 32)
C-Web@Ni-cotton supercapacitor fabric	Electrospinning	High – specialized equipment	275.8	1 mA cm^{-2} (GCD)	Huang *et al.* 2016 (ref. 27)
rGO/cotton yarn	Hydrothermal method	High – long processing time	9.54	0.06 mA cm^{-2} (GCD)	Li *et al.* 2023 (ref. 33)

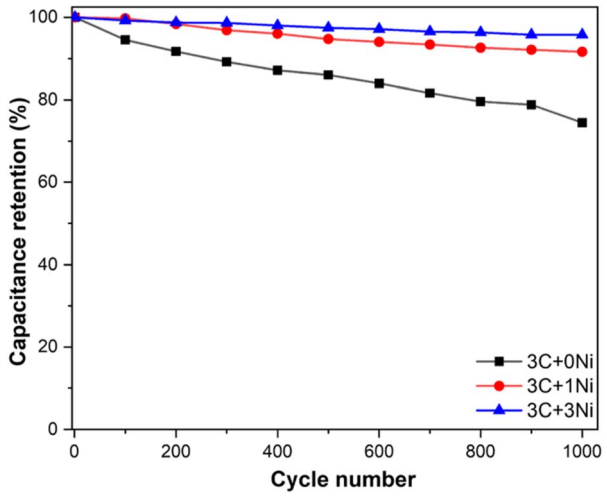

Fig. 7 Cyclic stability of the SCs with three AC immersions.

nickel deposition not only improves capacitance but also prolongs device lifespan.

Electrochemical impedance spectroscopy (EIS) analysis provides insight into the effect of nickel deposition on charge transfer and ion transport, as illustrated in Fig. 8. Fig. 8(a) illustrates the equivalent circuit model used to fit the EIS data. The equivalent circuit used for the fittings is the Randles circuit, which consists of a solution resistance (R_1) in series with the parallel combination of a constant phase element (CPE1), and the series combination of a Warburg impedance (W_1) and a resistance (R_2).[28] R_2 is depicted as a semicircle in the middle-frequency region, attributed to ionic accessibility in the pores or ion transport processes at the interface[29] or to the impedance between the electrode and current collector.[30]

CPE1 represents non-ideal capacitive behaviour, often used to model surface effects such as double-layer capacitance; meanwhile, W_1 represents the model diffusion processes in the system at low frequencies, as the inclination of the Nyquist plots of ~45° is an indication of semi-infinite length diffusion.[31]

A transmission line of semi-infinite length models the diffusion region, consistent with the high thickness of the cotton substrates (~300 mm).[34] For this equivalent circuit, we chose a finite-length Warburg element that represents a short circuit terminal (W_s element in ZView), whose finite-length Warburg impedance (Z_{FLW}) is calculated by: $Z_{FLW} = \frac{W_s - R \times \tan h\sqrt{W_s - Tj\omega}}{\sqrt{W_s - Tj\omega}}$, where $W_s - T = \frac{{L_D}^2}{D}$ and L_D is the thickness of the diffusion layer (cotton cloth), D is the diffusion coefficient, W_s–T is the diffusion time, and W_s–R is the Warburg resistance.[35]

In this case of $L_D \rightarrow \infty$, the Warburg impedance is in the form of semi-infinite Warburg diffusion,[36] as the electrolyte cannot penetrate to the bottom of the electrode. Fig. 8(b) shows the impedance spectra for samples without Ni (0Ni), and Fig. 8(c) shows the for samples with 1Ni, where the R_1 and R_2 values are smaller compared to Fig. 8(b), indicating lower solution and electrolyte/electrode resistances, respectively, which is in accordance with the results showed in a previous work,[14] probably caused by the change in the surface polarity as proposed by Tai *et al.*[22]

For C + 1Ni, 3C + 1Ni, and 1C + 5Ni SCs, the lowest R_2 is achieved when the smallest amount of Ni (1 min) is deposited. For higher Ni content, R_2 values are higher due to the aforementioned blocking effect in the carbon pores.

These R_2 values are consistent with the reported specific capacitances for both CV and GCD techniques, in which these electrodes presented the highest capacitances, as SCs with the lowest interfacial resistance between the electrode and the electrolyte[29] are also consistent with a previous work.[14] For higher Ni content, the blocking effect increases R_2, leading to a decrease in capacitance. For all the Ni contents (Fig. 8(b–f)), R_2 decreases with higher carbon immersions, representing lower composite resistance due to the larger active area resulting from the increased electrode–electrolyte contact area.[31] This results in improved pore accessibility and increased capacitance.

Electrodes with high micropore content and a poor pore conductivity network will lead to decreased ion efficiency, increasing the Warburg resistance.[35] More carbon immersions represent a high surface area and improve the presence of mesopores and micropores, which provide better accessibility of the electrolyte and reduce the Warburg resistance.Then, increasing the carbon content reduces the path length for electrolyte ions, thereby improving SC performance. Decreasing Warburg resistance enhances ionic accessibility in the bulk of the electrode and facilitates the formation of EDL capacitance within the pores.[29] This behaviour was observed in Table 5, where W_1–R and R_2 diminish for more AC ink immersions.

The exponent of the CPE element, which is denoted by eqn S6, represented in Table 5 as CPE-P, diminishes with the increment of carbon immersions for all the Ni concentrations. Although there is no consensus among researchers on the causes of the CPE-P change, it is argued that the increase in roughness and atomic-scale inhomogeneities causes the CPE-P (which is 1 for an ideal capacitor) to exhibit a higher deviation from unity.[37]

The impedance of the phase constant element is given by: $Z_{CPE} = \frac{1}{\text{CPE-T}(j\omega)^{\text{CPE-P}}}$, where Z_{CPE} is the impedance of the CPE, and CPE-T and CPE-P are the parameters that define CPE, where CPE-P is a dimensionless parameter that has values between 0 and 1, and signifies the degree of deviation from the vertical line in a Nyquist plot, meanwhile CPE-T is expressed in $Fs^{-}{}^{CPE-P-1}$ units.[38]

The assembly of a flexible SC prototype was carried out for 3C + 3Ni electrodes, for which 2 cm diameter electrodes and a cellulose membrane as a separator were used, with the difference that the electrolyte was KOH gel : PVA (1 : 1), which was encapsulated along with two aluminium foils used as current collectors inside a polypropylene encapsulation.[39] This device is shown in Fig. 9(a), demonstrating the physical flexibility of the supercapacitor under bending and its ability to maintain its structure under mechanical stress.

Fig. 9(b) shows the CV curves for the flexible SC in flat and bent states obtained at 100 mV s^{-1}, showing specific

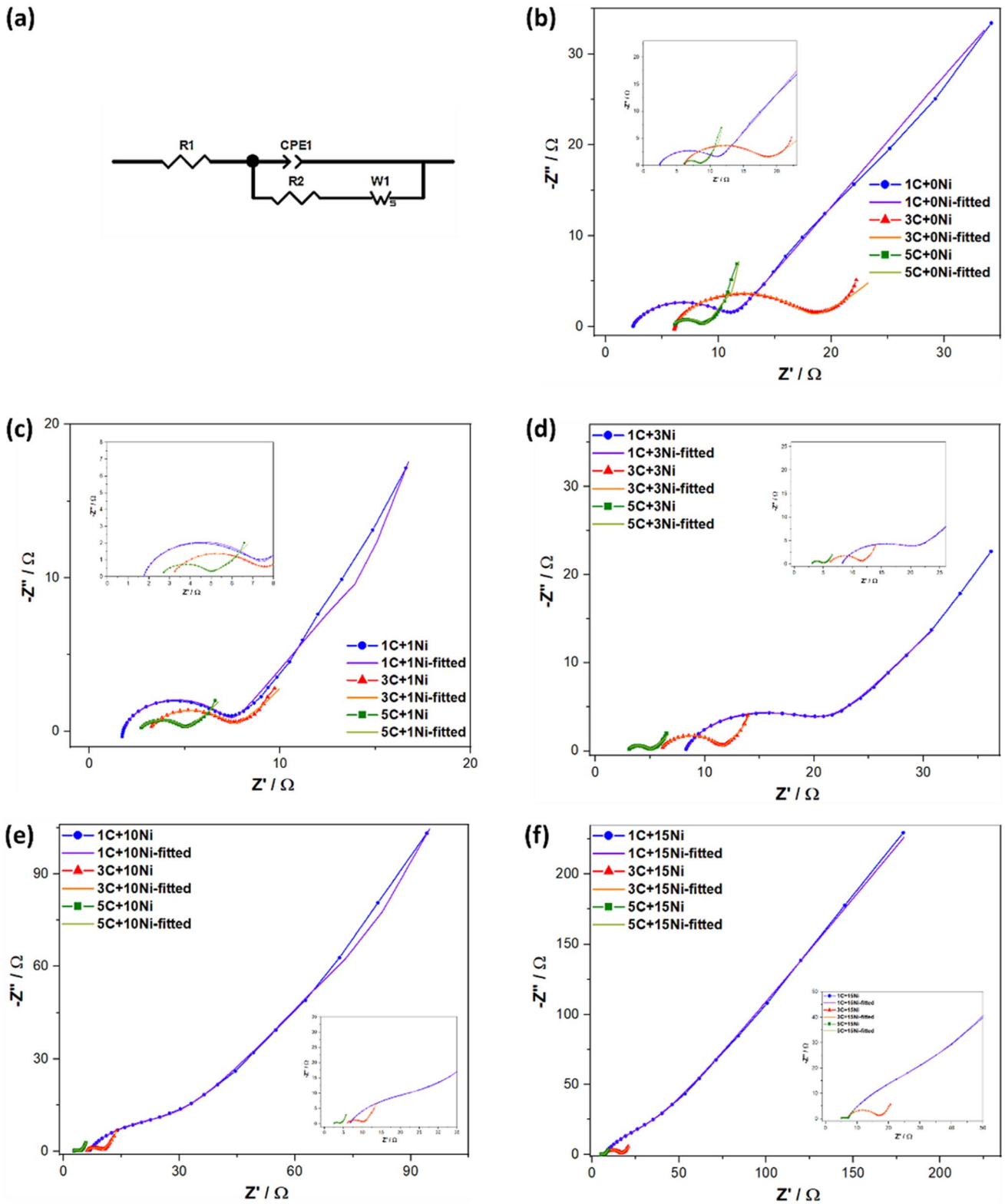

Fig. 8 EIS characterization: (a) equivalent circuit, and Nyquist plots of (b) 0Ni, (c) 1Ni, (d) 3 Ni, (e) 10Ni, and (f) 15Ni SCs.

capacitances of 10.48 mF cm^{-2} and 8.92 mF cm^{-2}, respectively. Illustrating that the device retains its electrochemical behavior under deformation, the minor differences between the flat and bent CV curves indicate good structural integrity and flexibility. Compared with the non-flexible SCs, the lower Cs are related to the poor contact between the electrodes and the current collectors, compared with the rigid cell of the non-flexible SCs.

Table 5 Parameters obtained in ZView simulation

	R_1 [W]	CPE-T [$Fs^{CPE-P-1}$]	CPE-P [–]	R_2 [W]	W_1–R [W]	W_1–T [s]	W_1–P [–]	C_s [mF cm^{-2}]
1C + 0Ni	1.77	0.000327	0.7622	9.15	44.92	7.14	0.6109	27.40
3C + 0Ni	5.99	0.000451	0.6875	6.42	22.08	19.52	0.4573	222.43
5C + 0Ni	5.63	0.003195	0.5544	3.26	18.87	19.98	0.6601	675.02
1C + 1Ni	1.72	0.000229	0.7982	5.64	50.84	7.56	0.6227	139.26
3C + 1Ni	3.03	0.001045	0.6956	4.46	10.57	12.80	0.5115	374.98
5C + 1Ni	2.50	0.001636	0.6660	2.53	7.31	12.55	0.5105	487.80
1C + 3Ni	8.12	0.001170	0.7087	13.14	80.32	9.94	0.5821	67.93
3C + 3Ni	5.85	0.000919	0.6841	5.77	12.50	8.46	0.5982	237.12
5C + 3Ni	2.75	0.001797	0.6057	2.33	6.65	11.0	0.5228	485.52
1C + 10Ni	6.53	0.001253	0.6572	28.06	387.3	9.16	0.5921	10.23
3C + 10Ni	5.73	0.001769	0.6207	4.57	19.04	7.35	0.6284	185.21
5C + 10Ni	2.28	0.005724	0.5424	2.01	8.80	7.39	0.6279	295.09
1C + 15Ni	7.12	0.000869	0.7475	33.64	824.30	8.38	0.5829	3.94
3C + 15Ni	6.82	0.000499	0.7618	9.92	22.05	11.28	0.5683	162.80
5C + 15Ni	4.57	0.005653	0.5352	2.31	10.60	7.15	0.5967	283.91

Fig. 9(c) shows the capacitance retention as a function of bending angle, where the device retains a high percentage of its initial capacitance even at large bending angles, highlighting its robustness under strain. Fig. 9(d) shows the capacitance retention as a function of the number of folding cycles, demonstrating the device's stability after multiple bending/

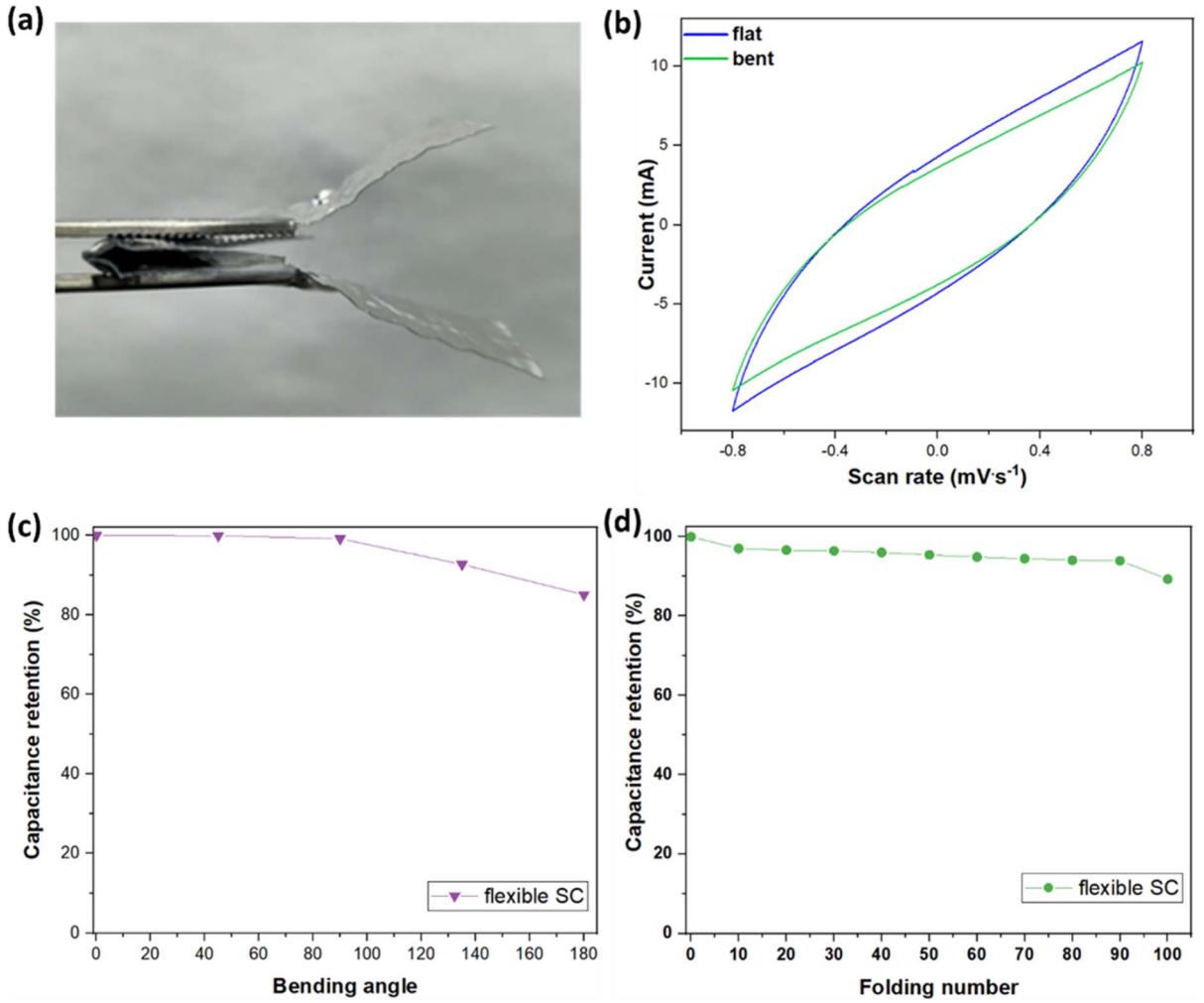

Fig. 9 (a) Photograph of the flexible supercapacitor, (b) cyclic volammetry of the flexible SC measured at 100 mV s^{-1}, (c) Capacitance retention characteristics of the flexible SC and (d) capacitance retention of the flexible SC after 100 folding times.

folding cycles, with minimal loss in capacitance. This durability is essential for applications requiring repeated mechanical flexing.

The lower specific capacitance observed in the flexible prototype compared to rigid cells is consistent with previous reports, in which polymeric gel electrolytes typically exhibit reduced ionic conductivity relative to liquid KOH due to restricted ion mobility within the polymer matrix.[40,41] Nevertheless, the gel provides essential advantages for wearable applications, including reduced leakage, mechanical flexibility, and durability under repeated deformation, as demonstrated in our bending and cycling experiments.

Compared to earlier reports on Ni–carbon textile supercapacitors, our approach offers three distinctive advantages. First, in terms of performance, the optimized cotton-based electrodes achieved areal capacitances up to 675.02 mF cm^{-2} (5C + 0Ni, GCD at 1.59 mA cm^{-2}) and 382.40 mF cm^{-2} (3C + 1Ni, CV at 5 mV s^{-1}), values that surpass many previously reported textile devices. Second, regarding cost and scalability, the fabrication relies solely on abundant cotton substrates, a simple dipping-impregnation process, and controlled sputtering, avoiding complex syntheses such as electrospinning or hydrothermal growth. Finally, in terms of methodological simplicity, the process requires minimal chemical reagents and can be readily scaled to large fabric areas, making it highly attractive for wearable and portable energy storage. These combined features distinguish our work from prior Ni–carbon textile electrodes and highlight its potential for practical, low-cost, and high-performance supercapacitors.

Conclusions

The results obtained in this work highlight the decisive influence of activated carbon content and nickel coating on the electrochemical performance of textile electrodes. Increasing the number of activated carbon immersions enhanced the active surface area by more than 90% (comparing electrodes with 1 and 5 immersions), leading to specific capacitances as high as 675.02 mF cm^{-2} (5C + 0Ni). While various fabrication strategies have been reported in the literature for flexible supercapacitors, many involve complex processes or high-cost equipment, we proposed a low-cost and facile approach—based on a simple dipping-impregnation method combined with controlled nickel sputtering—which offers a low-cost, scalable, and practical route for producing high-performance textile electrodes. This methodological simplicity, together with the excellent electrochemical performance and robust cycling stability demonstrated in this study, underscores the potential of these electrodes for integration into flexible and wearable energy storage systems.

A moderate nickel coating (0.002 g) was found to be crucial for improving conductivity and cycling stability, achieving 95.76% capacitance retention after 1000 cycles. However, thicker coatings led to pore blocking and reduced capacitance, confirming the importance of maintaining an optimal balance between carbon and nickel content.

Compared to more complex fabrication strategies, such as electrospinning or hydrothermal treatments, the method employed here—based on a simple dipping-impregnation process combined with sputtering on cotton—represents a low-cost, scalable, and practical route that leverages an abundant and inexpensive textile substrate. This methodological simplicity, together with the outstanding electrochemical performance and robust stability, positions these electrodes as a highly viable alternative for flexible textile supercapacitors.

Overall, the innovation of this work lies in demonstrating that low-cost materials and straightforward processes can compete with advanced technologies in terms of capacitance and durability. Thus, the development of these cotton–carbon–nickel electrodes opens new opportunities for portable, sustainable, and wearable energy storage systems.

Author contributions

Paola Vilchis-Gutiérrez: writing – original draft, investigation, methodology, data curation, conceptualization. José Ávila-Niño: validation, writing – review & editing, supervision, investigation, Dolores Durán-García: project administration, conceptualization, supervision, investigation. Marquidia Pacheco-Pacheco: supervision, investigation, data curation, Iván Martínez-Cienfuegos: review.

Conflicts of interest

There are no conflicts to declare.

Data availability

No primary research results, software or code have been included and no new data were generated or analysed as part of this paper.

Supplementary information (SI): which includes SEM/EDS micrographs and elemental mapping of Ni and C, together with galvanostatic charge–discharge curves of the supercapacitors under different immersion cycles and Ni deposition times. See DOI: https://doi.org/10.1039/d5ra09914e.

Acknowledgements

PGVG acknowledge Secihti for the phD grant 709996; we thank Dr Susana Gaucín (CIDETEQ) for obtaining SEM micrographs and EDS characterization, Dr Jannú Casanova (CIDETEQ) for technical support in magnetron sputtering, and Dr José Luis Herrera for technical support in obtaining film thicknesses.

Notes and references

1 M. Halper and J. Ellenbogen, *The MITRE Corporation*, McLean, Virginia, USA, 2006, pp. 1–29.
2 L. Li, Q. Zhong, N. D. Kim, G. Ruan, Y. Yang, C. Gao, H. Fei, Y. Li, Y. Ji and J. M. Tour, *Carbon*, 2016, **105**, 260–267.
3 Z. Wang, H. Wang, S. Ji, H. Wang, D. J. L. Brett and R. Wang, *J. Alloys Compd.*, 2020, **814**, 151789.

4 S. Xu, H. Hao, Y. Chen, W. Li, W. Shen, P. R. Shearing, D. J. L. Brett and G. He, *Nanotechnology*, 2021, **32**, 305401.
5 H. Zhang, C. Qi, X. J. Du, H. Zhang, Y. Zhang, T. Ma and Y. Sun, *Int. J. Hydrogen Energy*, 2019, **44**, 17544–17550.
6 J. P. Aguiar dos Santos, F. C. Rufino, J. I. Y. Ota, R. C. Fernandes, R. Vicentini, C. J. B. Pagan, L. M. Da Silva and H. Zanin, *J. Energy Chem.*, 2023, **80**, 265–283.
7 M. Pal and K. M. Subhedar, *Energy Storage Mater.*, 2023, **57**, 136–170.
8 S. Verma, A. Khosla and S. Arya, *J. Electrochem. Soc.*, 2020, **167**, 120527.
9 J. Gamby, P. L. Taberna, P. Simon, J. F. Fauvarque and M. Chesneau, *J. Power Sources*, 2001, **101**, 109–116.
10 D. Qu, *J. Power Sources*, 2002, **109**, 403–411.
11 G. H. Yuan, Z. H. Jiang, A. Aramata and Y. Z. Gao, *Carbon*, 2005, **43**, 2913–2917.
12 A. Burke, *Presented at STEPS Fall Symposium*, 2017.
13 P. Sundriyal and S. Bhattacharya, *Sci. Rep.*, 2020, **10**, 1–15.
14 P. G. Vilchis-Gutiérrez, J. A. Ávila-Niño, M. D. Durán-García and M. J. Pacheco-Pacheco, *Mater. Lett.*, 2024, **377**, 137401.
15 Y. Liu, X. Wang, K. Qi and J. H. Xin, *J. Mater. Chem.*, 2008, **18**, 3454–3460.
16 D. Islam, M. H. Uddin, B. Pan and M. M. A. Joy, *Chem. Phys. Lett.*, 2020, **760**, 138007.
17 Q. Zhou, X. Ye, Z. Wan and C. Jia, *J. Power Sources*, 2015, **296**, 186–196.
18 M. Pasta, F. La Mantia, L. Hu and Y. Cui, *Nano Res.*, 2010, **3**, 452–458.
19 S. Byun and J. Yu, *J. Power Sources*, 2016, **307**, 849–855.
20 S. Lowell, J. E. Shields, M. A. Thomas and M. Thommes, *Characterization of Porous Solids and Powders: Surface Area, Pore Size and Density*, Springer Netherlands, Dordrecht, 1st edn, 2004, p. 16.
21 *Handbook of Nanocomposite Supercapacitor Materials I*, ed. K. K. Kar, Springer, 2020, DOI: 10.1007/978-3-030-52359-6.
22 Y. L. Tai and H. Teng, *Carbon*, 2004, **42**, 2335–2338.
23 F. Liu, Y. Lai, J. Liu, B. Wang, S. Kuang, Z. Zhang, J. Li and Y. Liu, *J. Alloys Compd.*, 2010, **493**, 305–308.
24 N. H. Basri, M. Deraman, M. Suleman, N. S. M. Nor, B. N. M. Dolah, M. I. Sahri and S. A. Shamsudin, *Int. J. Electrochem. Sci.*, 2016, **11**, 95–110.
25 M. Liu, L. Gan, W. Xiong, F. Zhao, X. Fan, D. Zhu, Z. Xu, Z. Hao and L. Chen, *Energy Fuels*, 2013, **27**, 1168–1173.
26 J. Li, E. Liu, W. Li, X. Meng and S. Tan, *J. Alloys Compd.*, 2009, **478**, 371–374.
27 Q. Huang, L. Liu, D. Wang, J. Liu, Z. Huang and Z. Zheng, *J. Mater. Chem. A*, 2016, **4**, 6802–6808.
28 J. Mainka, W. Gao, N. He, J. Dillet and O. Lottin, *Electrochim. Acta*, 2022, **404**, 139740.
29 H. D. Yoo, J. H. Jang, J. H. Ryu, Y. Park and S. M. Oh, *J. Power Sources*, 2014, **267**, 58–67.
30 T. S. Mathis, N. Kurra, X. Wang, D. Pinto, P. Simon and Y. Gogotsi, *Adv. Energy Mater.*, 2019, **9**, 1902007.
31 V. Sunil, B. Pal, I. I. Misnon and R. Jose, *Mater. Today: Proc.*, 2021, **46**, 1588–1594.
32 K. Jost, C. R. Perez, J. K. McDonough, V. Presser, M. Heon, G. Dion and Y. Gogotsi, *Energy Environ. Sci.*, 2011, **4**, 5060–5067.
33 L. Li, D. Du, C. He, L. Yu, W. Tang, S. Hu, X. Wang, Z. Fu, L. Xia, W. Xu and L. Kong, *Ind. Crops Prod.*, 2023, **205**, 117547.
34 A. C. Lazanas and M. I. Prodromidis, *ACS Meas. Sci. Au*, 2023, **3**, 162–193.
35 I. I. Misnon, N. K. M. Zain, R. A. Aziz, B. Vidyadharan and R. Jose, *Electrochim. Acta*, 2015, **174**, 78–86.
36 T. Q. Nguyen and C. Breitkopf, *J. Electrochem. Soc.*, 2018, **165**, E826–E831.
37 Z. Kerner and T. Pajkossy, *J. Electroanal. Chem.*, 1998, **448**, 139–142.
38 A. Lasia, *J. Phys. Chem. Lett.*, 2022, **13**, 580–589.
39 M. Fu, R. Lv, Y. Lei and M. Terrones, *Small*, 2021, **17**, 2004827.
40 G. Behzadi Pour, H. Nazarpour Fard and L. Fekri Aval, *Gels*, 2024, **10**, 803.
41 H. Ur-Rehman, A. Shuja, M. Ali, M. S. Khan, I. Murtaza and H. Meng, *J. Mater. Sci.: Mater. Electron.*, 2022, **33**, 2322–2335.